

# An unified model for superluminal motion and state transition on microquasars and quasars

B.P. Gong<sup>1,2</sup>

## ABSTRACT

Superluminal motion has been interpreted as relativistically moving out flow. The increasing observations of such sources provide chance to investigate their mechanism in detail. This paper proposes that superluminal motion may be jet precession induced blob motion. This model can interpret a number of observational phenomena which are not well understood under the scenario of bulk motion, such as the absence of the receding blob after the outburst and the receding blob becomes brighter than the approaching one in XTE J1550-564 . Moreover the compton scattering of photos from a warped accretion disk may form a structured jet. And the precession of the structured jet may lead to the complicated state transitions observed in microquasars like GRS 1915+105. Applying to AGNs, the model may explain the scales of length and time of the phenomena proportioning to the mass of the black hole. The new model can be tested easily on microquasars, i.e., XTE J1550-564, on which the previous receding blob should move towards the core instead of away from it after 2002, and the previous approaching blob shall disappear.

*Subject headings:* radio continuum: stars–stars: individual (GRS 1915+105, XTE J1550-564)– X-rays: stars

## 1. Introduction

The appearance on the sky of relativistically moving out flow, which expands at speed greater than the speed of light has

been predicted by Rees (1966) five years in advance of the discovery of superluminal motion (Whitney et al 1971; Cohen et al 1971).

The apparent velocity of separation is the ratio of the difference in observed positions to the observed time-interval. Suppose that at  $t = 0$  in our frame, the moving blob is at the original point, a distance  $D$  away from us, and sends us a signal. That signal arrives at the time

---

<sup>1</sup>Centre d'Etude Spatiale des Rayonnements, CNRS-UPS, 9, avenue du Colonel Roche, 31028 Toulouse Cedex 4, France

<sup>2</sup>Department of Physics, Huazhong University of Science and Technology, Wuhan 430074, P.R. China

$D/c$ . After time  $\Delta t$  in our frame, the moving blob has moved a distance  $v\Delta t \sin \theta$  in the transverse direction and sends us a second signal. This one arrives at  $t = \Delta t + D/c - (v/c)\Delta t \cos \theta$ . Thus the apparent transverse velocity is,

$$v_a = \frac{v \sin \theta}{1 - \frac{v}{c} \cos \theta}, \quad (1)$$

when  $v \sim c$  and  $\theta \sim 0$ ,  $v_a \sim 2c/\theta$ , which can be as large as 10 times the speed of light, as shown in Fig. 1a.

The first superluminal source discovered in our galaxy was GRS 1915+105 a recurrent transient source of hard X-ray found by Castro-Tirado et al 1994. Soon after similar phenomenon was observed by two different groups GRO J1655-40 (Zhang et al 1994), XTE J1748-288 (Smith et al 1998). These galactic source are called microquasars in which the Black Hole (BH) is only a few solar masses instead of several million solar masses as in the case of quasars.

Mirabel et al (1994) observed with the very Large Array (VLA) four ejection events of radio-emitting clouds from the high energy source GRS 1915+105. Who also noted small apparent changes in the projection of the jets on the sky (Rodrguez & Mirabel 1999).

Fender et al. (1999) reported observations of a major outburst with the Multi-Element radio Linked Interferometer Network (MERLIN), which is five times the angular resolution of the VLA at 5 GHz. These observations revealed again relativistic ejections, but with higher (by approximately 20%) proper motion than those measured with VLA.

Miller-Jones et al. (2005) reported two

separate outbursts in 2001 March and 2001 July. As the former observations, no deceleration is observed in GRS 1915+105. Liner polarization is observed in the approaching jet component, with a gradual rotation in position angle and a decreasing fractional polarization with time. These observations are difficult to understand under the scenario of bulk motion.

On the other hand, there are striking similarities between GRS 1915+105 and the SS 433 (Rodrguez & Mirabel 1999), in which the jet precession scenario has been widely accepted.

This paper suggests that superluminal motion on microquasars like GRS 1915+105 may also be an effect of jet precession, differing from SS 433 only on the misalignment angle between the jet axis and Line of Sight (LOS). In the precession of SS 433, the angle between the jet axis and LOS is relatively larger, whereas, in GRS 1915+105, the jet axis precesses across the LOS, as shown in Fig. 2a. The jet precession model can interpret following phenomena:

(a) why the ratio of the displacement of the approaching blob to the receding blob is not a constant.

(b) why the receding jet appears later than the approaching jet in XTE J1550-564 (for year).

(c) why the position angle changes  $\sim 10\text{deg}$  in 20-30-d in GRS 1915+105.

(d) why there is obvious oscillation in the receding blob.

(e) why 20% discrepancy in proper motion between the ejection of 1994 and 1997.

(f) why deceleration appeared in XTE J1550-564 but not in GRS 1915+105.

(g) why the decrease in flux density with angular separation from the core on GRS 1915+105 is remarkably similar with that of SS 433.

Thanks to the rapid jet precession in microquasars, the new model can be tested easily, i.e., the return of the approaching of GRS 1915+105 should be observed in around one year after each major outburst.

Microquasar XTE J1550-564 may already reverse its approaching and receding blob through precession, hence the previously receding blob should move towards the core after 2002. Correspondingly the Doppler-shift feature of XTE J1550-564 in year 2002 should have opposite sign comparing with that of year 2000.

Jet precession induced blob motion may explain the superluminal motion. Moreover, the precession and nutation of a structured jet can interpret the state transition and oscillation observed in microquasars like GRS 1915+105.

## 2. The model

The jet-disk interaction is still an open question. In this paper we assume that the precession of the accretion disk causes the change of the jet axis. Consequently the jet axis varies relative to LOS.

Similar as SS433, the jet precesses in certain half-opening angle cone, the individual jet components move ballistically away from the system (Migliari et al 2005). The direction in which the blobs are observed to moving match the direction of the jets at the time when the blobs were just forming. And the travel direction of the blobs may indicate the average phase angle of the jet during the time of their for-

mation (Dunn et al 2006). Therefore, the length of the blobs to the core is approximately a constant by assuming an approximately equal ISM density around a microquasar.

With  $D_0$  the distance of the observer to the approaching blob (when the position angle  $\theta = 0$ ), the instantaneous distances of the approaching and receding blobs relative to the observer are given

$$D_a = D_0 + l_0 \sin \lambda [1 - \cos \theta_a], \quad D_r = D_0 + l_0 \sin \lambda [1 + \cos \theta_r], \quad (2)$$

where  $\theta_a \equiv \theta(T_a)$  is the misalignment angle between the axis of the approaching jet and LOS, and  $\theta_r \equiv \theta(T_r)$  corresponds to that of the receding jet (note  $\theta_r$  and  $\theta_a$  denote absolute values). In which  $T_a$  and  $T_r$  are the time of arrivals of the two blobs in observer's frame,  $l_0$  is the distance from the core to each blob, and  $\lambda$  is the misalignment angle between the jet axis and the orbital angular momentum vector,  $\mathbf{L}$ , as shown in Fig. 1b.

The blobs appeared to move away from the core. The separation of the approaching and receding blobs measured by the observer are given by,

$$R_a = l_0 \sin \lambda \sin \theta_a, \quad R_r = l_0 \sin \lambda \sin \theta_r, \quad (3)$$

The angles,  $\theta_a$  and  $\theta_r$  can be denoted by  $\theta$ , which varies with the precession of the jet axis (Dunn et al 2006),

$$\cos \theta = \cos i \cos \lambda + \sin i \sin \lambda \cos \eta, \quad (4)$$

where  $i$  is the orbital inclination angle. And  $\eta = \dot{\Omega}_1 t + \eta_0$  is the precession phase of the jet axis, in which  $\dot{\Omega}_1$  is the precession frequency of accretion disk by (Katz 1997),

$$\dot{\Omega}_1 = -\frac{3}{4} \frac{Gm_2}{a} \left(\frac{a_d}{a}\right)^2 \frac{\cos \lambda}{(Gm_1 a_d)^{1/2}}, \quad (5)$$

where  $m_1$  and  $m_2$  are the masses of the accreting object and the companion star respectively,  $a$  and  $a_d$  are the separation of the two bodies and the disk radius respectively.

Actually Eq. (5) is equivalent to a general expression, Eq. (47) of Barker and O’Connell (1975), which can be understood as a result of perturbation by the mass distribution of the disk to the classical gravitational two-body problem. The perturbation also affects the six orbital elements,  $i$ ,  $e$ ,  $a$ ,  $\Omega$ ,  $\omega$ ,  $P_b$ . In which  $e$  is the eccentricity of the orbit,  $P_b$  is the orbital period,  $\omega$  is the longitude of the periastron, and  $\Omega$  is the longitude of the ascending node, as shown in Fig. 3.

The precession of the disk results the precession of the orbital plane, therefore, the ascending node is not at static with respect to the LOS, thus  $i$  in Eq. (4) is a function of time,

$$\cos i = \cos I \cos \lambda_{LJ} + \sin I \sin \lambda_{LJ} \cos \Omega, \quad (6)$$

where  $I$  is the misalignment angle between the total angular momentum and LOS, and  $\lambda_{LJ}$  is the misalignment angle between  $\mathbf{L}$  and  $\mathbf{J}$ , as shown in Fig. 3.

The general expression of  $\dot{\Omega}$  is given by Barker & O’Connell (1975), the magnitude of which along the total angular momentum is given (Wex & Kopeikin 1999),

$$\dot{\Omega} = \frac{3}{4} \frac{GmJ_2}{a^5(1-e^2)^2} \frac{P_b \sin 2\lambda}{2\pi \sin \lambda_{LJ}}, \quad (7)$$

where  $J_2 = (I_3 - I_1)/m_d$  ( $I_3$  is the principal moment of inertia of the disk,  $I_1$  is the moment of inertia with respect to an arbitrary axis, and  $m_d$  is the disk mass).

Notice that  $\dot{\Omega}$  can be larger than  $\dot{\Omega}_1$ . Thus the variation of  $\theta$  depends not only

on the precession phase,  $\eta$  of Eq. (4), but also on the rapid variation of the orbital inclination angle,  $i$ , induced by  $\dot{\Omega}$  of Eq. (7). The precession of  $\eta$  denotes the precession of jet along the precession cone with opening angle  $\lambda$  at time scale, i.e., years, and the variation of  $i$  leads to a nutation with much smaller opening angle, and at shorter time scale, as shown by the small solid ellipse in Fig. 2a.

### 3. Application to super luminous motion

By the given orbital parameters  $P_b = 33.5 \pm 1.5$ -d,  $m_1 = 14 \pm 4M_\odot$ ,  $m_2 = 1 - 1.5M_\odot$  (Fender & Belloni 2004), we have  $a = 8 \times 10^{12}$ cm. And assuming  $a_d = a/2$  and  $\lambda = \pi/6$ , obtains,  $\dot{\Omega}_1 \sim 0.26$ deg day $^{-1}$  by Eq. (5). In such case the period of  $\eta$  is approximately  $\sim 2\pi/\dot{\Omega}_1 \approx 3.8$  yr.

If the outbursts correspond to  $\theta \sim 0$  (the jet axis is approximately aligned with LOS), as shown in Fig. 2b, then the 3.8yr period of the jet precession implies that the outbursts of GRS 1915+105 in January 1994 (Mirabel & Rodriguez 1994), October 1997 (Fender et al 1999) and July 2001 (Miller-Jones et al 2005) correspond to the beginning ( $\theta \sim 0$ ) of three different period of jet precessions respectively.

Note that when the parameter, i.e.,  $a_d$  increases, the 3.8yr periodicity can still hold by assuming  $\lambda > \pi/6$ .

#### 3.1. The long-term effects

As the bulk motion model, the jet precession model also corresponds to different velocities of the approaching and receding blobs. However these two models predict different behavior on the ratios of the dis-

placement of the approaching blob to the receding blob. Moreover the two models also correspond to different evolution on the flux density of the approaching and receding blobs.

By the jet precession scenario, the speed of the blobs measured in a frame at rest to the core is  $V_0 = l_0 \dot{\Omega}_1 \sin \lambda$ . The time measured in the observer's frame is  $T$ , while in the frame at rest to the moving blob, the corresponding time is  $t$ , they are related by,

$$T = \frac{t + Vx/c^2}{(1 - V^2/c^2)^{1/2}} . \quad (8)$$

Putting  $V = V_0 \sin \theta$ ,  $x = l_0(1 - \cos \theta) \sin \lambda$ , and  $t = \theta_0/\dot{\Omega}_1$  into Eq. (8),  $T_a$ , the time takes for the approaching blob moving from  $\theta = 0$  to  $\theta = \theta_0$  is obtained. Similarly by putting  $x = l_0(1 + \cos \theta) \sin \lambda$  and  $t = \theta_0/\dot{\Omega}_1$  into same equation, we actually obtain  $T_r$ , the time taken for the receding blob rotating by the same angle,  $\theta$ , as the approaching one. Then following relation is obtained,

$$T_a > t > T_r . \quad (9)$$

By Eq. (9) and Eq. (4), the observer on the earth will tell that  $\theta_a > \theta_r$ , and hence we have  $R_a > R_r$  by Eq. (3).

In observer's reference frame, the time interval between the two signals sent by the approaching blob at the moment,  $\theta = 0$  and  $\theta = \theta_0$ , is given

$$\delta T_a = T_a + l_0(1 - \cos \theta_a) \sin \lambda / c . \quad (10)$$

Notice that when  $\theta = 0$ , the blob is at the position which closest to the observer, as shown in Fig. 1b. Similarly time interval for the receding blob is

$$\delta T_r = T_r + l_0(\cos \theta_r - 1) \sin \lambda / c . \quad (11)$$

Therefore, the apparent transverse velocities of the two blobs,  $v_a = R_a/\delta T_a$  and  $v_r = R_r/\delta T_r$ , can be obtained respectively. Obviously, we have

$$v_a \sim v_r \sim V_0 , \quad (12)$$

Consequently, if  $V_0 \leq c$ , then  $v_a$  and  $v_r$  should be less than the speed of light also.

However if an observer treats the signal sent by the approaching blob at  $\theta = 0$  as from the core of the microquasar instead of the from the position which is closest to the observer, as shown in Fig. 1, then the time interval corresponding to Eq. (10) is  $\Delta T'_a = T_a - l_0(\cos \theta_a - 1) \sin \lambda / c$ . And the corresponding apparent transverse velocity is  $v'_a = R_a/\Delta T'_a > v_a$ , and hence  $v'_a > c$  is possible. In other words, jet precession induced blob motion may appear as superluminal motion.

Moreover,  $\theta_a$  and  $\theta_r$  are different functions of time, and by Eq. (3),  $R_r/R_a$  is also a function of time. Therefore the jet precession model predicts a variable  $R_r/R_a$ .

Comparatively the bulk motion model predict that  $R_r/R_a = 1 - 2V_0 \cos \theta / c$ , which is a constant, since the position angle  $\theta$  and the velocity  $V_0$  are constants. The observations (Mirabel & Rodriguez 1994; Fender & Belloni 2004; Miller-Jones et al 2005) likely support a variable  $R_r/R_a$ .

Owing to Doppler deboosting of the receding jet flux density,  $\theta_r = 0$  corresponds to the minimum flux density. As  $\theta$  increases the flux density increases, in the case  $\theta_r > \theta_{cr}$  ( $\theta_{cr}$  denote a critical angle), the receding jet can be luminous enough to be observed. This explains the absence of X-ray emission in the receding blob after the outburst in XTE J1550-564 (Corbel et al 2002). Whereas in the bulk motion

scenario, the absence of the receding blob is not expected, since it should be brighter where it is near the core instead of far away from the core.

The superluminal motion of GRS 1915+105 observed in radio band may be dominated by the emission from the condensations instead of the beam, therefore the effects of Doppler boosting and deboosting are not as obvious as that of X-ray emission of XTE J1550-564.

Assuming  $V_0 = 0.9c$ , we have  $l_0 = V_0/(\dot{\Omega}_1 \sin \lambda) \sim 6000\text{mas}$ . Therefore, the displacement varies with  $\eta$  at a rate,  $l_0 \dot{\Omega}_1 \sin \lambda \sim 14\text{mas/day}$ .

The major radio flare of XTE J1550-564 in September 1998 corresponds to the time that the eastern jet (approaching jet) towards LOS. The observations of June, August and September 2000 correspond to the increasing of  $\theta$ . The observations of March 2002 and June 2002 show that the western (receding) blob became much brighter than the eastern (approaching) blob (Corbel et al 2002). This implies  $\theta > \pi/2$  in 2002, in other words the receding blob became the approaching one.

Therefore the transition ( $\theta = \pi/2$ ) should happen in 2001, which implies a period of precession of  $\sim 12\text{yr}$  ( $\theta \sim 0$  in September 1998, and  $\theta \sim \pi/2$  in 2001). This prediction can be tested by further observation of XTE J1550-564. The next evolution would be the disappearance of the eastern blob and the displacement of the western blob would be closer to the core than that in March 2002 and June 2002. Owing to the increasing Doppler boosting the western blob should be brighter and brighter until the next outburst.

Two separate outbursts in 2001 March and 2001 July on GRS 1915+105 are observed (Miller-Jones et al 2005). As the former observations, no deceleration is shown in GRS 1915+105. Whereas in XTE J1550-564 deceleration has been observed (Corbel et al 2002).

This is because most observations of GRS 1915+105 last a few months after an outburst, which corresponds to a relatively small position angle variation,  $\theta \sim \pi/10$ . Whereas, the observation of XTE J1550-564 in 2002 corresponds to  $\theta \geq \pi/2$ . Therefore, XTE J1550-564 has passed the deceleration regime, whereas GRS 1915+105 actually has not. The observation of GRS 1915+105 of 1995 August 10 could have measured the return of the approaching blob, however it is unreliable since the individual condensations were resolved only in one epoch (Rodríguez & Mirabel 1999).

### 3.2. The short-term effects

The precession of the jet is actually a short-term nutation superimposed on the long-term primary precession. The short-term nutation corresponds to a variation of the position angle at the time scale of the orbital period, and the amplitude of which is much smaller than that of the primary precession.

By the orbital parameters we have the orbital angular momentum,  $L \sim 4 \times 10^{53} \text{g cm}^2 \text{s}^{-1}$ .

Assume that the mass of the ring (at radius  $a_d = a/2$ ) is  $0.1M_\odot$ , which corresponds to an angular momentum of  $L_d \sim 2 \times 10^{52} \text{g cm}^2 \text{s}^{-1}$ . Thus the ratio of spin angular momentum of the binary system to the orbital angular momentum of the

binary is  $S/L \sim 5 \times 10^{-2}$ . Thus the misalignment angle,  $\lambda_{LJ} \sim S/L \sim 5 \times 10^{-2}$ , and hence the orbital inclination angle  $i$  of Eq. (6) and in turn  $\theta$  of Eq. (4) can vary at the amplitude  $\delta\theta \sim 5 \times 10^{-2}$  rad.

Inputting the orbital parameters (assuming  $e = 0$ ) into Eq. (7), the precession rate of the orbital plane can be obtained,  $\dot{\Omega} \approx 4.4 \times 10^{-6} \text{s}^{-1}$ , which corresponds  $2\pi/\dot{\Omega} \sim 4P_b/5$ , and at an amplitude,  $\sim 5 \times 10^{-2}$  rad.

The periodicity of  $P_b/2$  has been found in SS433, by the spectral lines, which is interpreted as the nodding motion of accretion rings and disks (Katz et al 1982). This paper proposes an alternative interpretation to the similar periodicity,  $4P_b/5$  in GRS 1915+105, which is induced by the rapid precession of the orbital plane ( $\dot{\Omega}$ ) instead of the disk.

Therefore, we have variation of  $\theta$  induced by  $\Omega$  at a period  $\sim 4P_b/5$ . And since  $\dot{\Omega}$  and  $\lambda_{LJ}$  are function of the orbital phase, the variation of  $\theta$  also has a period  $P_b$ . So  $\theta$  can vary at the short time scales,  $\sim 4P_b/5$  and  $\sim P_b$ .

The observation of GRS 1915+105 in March 2001 (Miller-Jones et al 2005) shows only a single northwestern component (receding), which vibrates back and forth. The displacement from the core increases and decreases rapidly and at large amplitude. Simultaneously three distinct southeastern components (approaching) were seen to be ejected.

The three distinct approaching components can be interpreted as multi ejections in the bulk motion scenario. Due to the Doppler boosting, the weak components in the approaching ejectors can be observed, whereas that of receding ones are unob-

servable owing to the Doppler deboosting. However the vibration of the single receding component is still difficult to understand.

By the jet precession model the three distinct approaching ejectors might be the blob just forming plus the ones that are the remnants of earlier generations of bubbles. Owing to the Doppler boosting of the jet flux density, the low-temperature whorl can be observed, and the remnant of earlier generations of bubbles might mimic different ejections.

For the receding blob, the Doppler deboosting in the receding jet flux density makes the remnants unobservable. And thus the appearance is the oscillation of a single receding component (just formed).

The primary precession changes  $\theta$  at a rate approximately  $\sim 0.26 \text{deg day}^{-1}$ , hence in 20-30-d, the position angle changes  $\sim 5 - 8 \text{deg}$ . And consider the contribution by the nutation of  $\sim 3 \text{deg}$ , the 10 deg variation on the position angle (Rodríguez & Mirabel 1999) is possible.

If the opening angle of the emission beam is around 10deg, then it would take  $10/0.26 = 38.5\text{-d}$  for the beam sweeping through LOS by the primary precession ( $\eta$ ). However, due to the change in  $\theta$  caused by the short-term effects, the beam can pass through LOS before and after the primary passing process. In other words, the actual time of sweeping is approximately three times of 38.5-d, which is  $\sim 116\text{-d}$ . This explains why outburst of GRS 1915+105 lasts 3-4 months.

In one period of  $\theta$ , i.e., from March 1994 to October 1997,  $\theta$  may vary at an amplitude of  $\theta \sim 5 \times 10^{-2}$  by short-term effects.

The total change of  $\theta$  by the primary precession in one period is  $\sim 1$  rad. Thus we have  $\delta\theta/\theta \sim 10^{-1}$ , and by Eq. (3), the discrepancy in the proper motion at level 10% – 20% (Mirabel & Rodriguez 1994; Fender et al 1999) can be explained.

GRS 1915+105 and SS 433 show similar decrease in flux density with angular separation from the core (Rodríguez & Mirabel 1999). By the jet precession model, after the outburst, the position angle of GRS 1915+105 may close that of SS433. And due to the jets are produced by the same physics, hence similar decrease in flux density with angular separation is expected.

#### 4. The state transition of GRS 1915+105

The superluminal motion of GRS 1915+105 is the effect of jet precession with position angle,  $\theta > 0$ , the state transition of it corresponds to the precession in the case both  $\theta > 0$  and  $\theta \sim 0$ . The precession of a structured jet may be responsible for the complicated state transitions in GRS 1915+105.

The behavior on light-curves, color-color diagrams, and color-intensity diagrams can be described by state A, state B, and state C (Belloni et al 2000). States A and B corresponds to soft energy spectra with an observable inner region of the accretion disk, whereas state C is related to the low state (Belloni et al 1997a,b).

As in AGNs, microquasars should also have a compact radio core corresponding to the state, say C1, which forms to the innermost cone of the structured jet.

The compton scattering of accretion disk photos by relativistic nonthermal elec-

trons in the jet have been used to explain the high-energy gamma radiation from extragalactic radio sources (Dermer 1992).

Koerding et al (2002) point out that if the emission is relativistic beamed then the high X-ray luminosity of an increasing number of X-ray sources in nearby galaxies can be explained in the case of BH mass less than  $10M_{\odot}$ .

Similarly the scattering of the photos from the inner region of the disk in microquasars may produce beamed radiation and hence form cones around the compact radio core, which correspond to high/soft states A and B.

The inner disk may be warped like Fig. 4, which may be responsible for the discrepancy in state A and B. As shown in Eq. (5), the outer region of the accretion disk precesses more rapidly than that of the inner one. The precession propagates into the inner region through viscosity, which may contribute to the warping of the accretion disk.

On the other hand, outside the cones of states A and B is the state C2, which is an intermediate state transforming from the beamed to unbeamed state. State C2 is represented by the large green cone in the structured jet as shown in Fig. 4.

As the angle  $\theta$  further increases the beamed radiation reduces substantially. The emission received may be from the tilted disk, the corona, wind from the companion star, as well as the side of the jets, which is much fainter than that of the beamed one and state C2. This low state may correspond to C3. Apparently rapid variabilities can only be produced in the beamed states (A and B), instead of unbeamed ones.



In most of time the jet axis is not aligned with LOS, so the luminosity is low (C3), which corresponds to state (i) (Fender & Belloni 2004), as shown in Fig. 5. As the precessing of the jet axis, the LOS is gradually close the jet axis, the luminosity increases, thus one observes state C2 (bright) corresponding to state (ii) (Fender & Belloni 2004).

As the jet precession continues, one would observe the state series, A, C1, A, B, and C2, as shown in Fig. 4.

However due to the short-term effect, the structured jet may repeat the state series to the observer. This explains the oscillation in the state transition (Fender & Belloni 2004).

The short-term effect in the case of low state cannot make significant variation in the emission, but it changes position angle and vibrates the blobs as discussed in Section 3.2. Therefore the oscillation in the high state and at the low state may be caused by the same effect of the jet axis at different angle relative to LOS.

## 5. Application to AGNs

In the case of a quasar the separation of the two blobs is of several million light years instead of a few light years as in microquasars. And the mass of black hole is of several million solar masses instead of a few solar masses as in microquasars.

Assuming  $P_b = 10\text{yr}$ ,  $a_d = 1 \times 10^{15}\text{cm}$ ,  $m_1 = m_2 = 1 \times 10^6 M_\odot$ , and through Eq. (5),  $\dot{\Omega}_1 \sim 1 \times 10^{-14}\text{rad s}^{-1}$  is obtained. In such case, we have the speed of the two blobs,  $v \sim l_0 \sin \lambda \dot{\Omega}_1 \sim c$ , when  $l_0 \sim 10^6\text{ly}$ . If the opening angle of the beam is also 10 deg, then it would take  $\sim 6 \times 10^5\text{yr}$  for the

quasar to sweep through LOS.

Therefore, the scales of length and time of the phenomena are proportional to the mass of the BH.

Microquasars and quasars contain three basic ingredient, a black hole, an accretion disk heated by viscous dissipation, and collimated jets of high energy particles (Mirabel & Rodriguez 1998). By an universal mechanism for microquasars and quasars, if the LOS is aligned with the eject matter (which can eject many times) of microquasars and quasars, then microblazar and blazar can be observed respectively (Mirabel & Rodriguez 1998).

By the jet precession model, the jet is a steady out flow, microblazar and blazar are temporary states of microquasar and quasar respectively. When the jet axis is aligned with LOS through precession, microblazar and blazar are observed; and when the jet axis precesses away from LOS, quiescent state is seen, which can be shown in Fig. 4.

## REFERENCES

- Barker, B.M. & O'Connell, R.F., 1975, Phys. Rev. D., 12, 329.
- Belloni, T., Klein-Wolt, M., Mendez, M., vanderKlis, M., & vanParadijs, J., 2000, A&A, 355, 271.
- Belloni, T., Mendez, M., King, A.R., vanderKlis, M., & vanParadijs, J., 1997, ApJ, 488, 109.
- Belloni, T., Mendez, M., King, A.R., vanderKlis, M., & vanParadijs, J., 1997, ApJ, 479, 145.
- Castro-Tirado, A.J., Brandt, S., Lund,

- N., Lapshov, I., Sunyaev, R.A., Shlyapnikov, A.A., Guziy, S., & Pavlenko, E.P., 1994, *ApJS*, 92, 469.
- Corbel, S., Fender, R.P., Tzioumis, A.K., Tomsick, J.A., Orosz, J.A., Miller, J.M., Wijnands, R., & Kaaret, P., 2002, *Sci*, 298, 196.
- Cohen, M.H., Cannon, W., Purcell, G.H., Shaffer, D.B., Broderick, J.J., Kellermann, K.I., & Jauncey, D.L., 1971, *ApJ*, 170, 207.
- Dermer, C.D., Schlickeiser, R., & Mastichiadis, A., 1992, *A&A*, 256, 27.
- Dunn, R.J.H., Fabian, A.C., & Sanders, J.S., 2006, *MNRAS*, 366, 758.
- Fender, R., & Belloni, T., 2004, *ARA&A*, 42, 317.
- Fender, R.P., Garrington, S.T., McKay, D.J., Muxlow, T.W.B., Pooley, G.G., Spencer, R.E., Stirling, A.M., & Waltman, E.B., 1999, *MNRAS*, 304, 865.
- Katz, J.I., 1997, *ApJ*, 478, 527.
- Katz, J.I., Anderson, S.F., Grandi, S.A., & Margon, B., 1982, *ApJ*, 260, 780.
- Koerding, E., Falcke, H., Markoff, S., 2002, *A&A*, 382, 13.
- Miller-Jones, J.C.A., McCormick, D.G., Fender, R.P., Spencer, R.E., Muxlow, T.W.B., & Pooley, G.G., 2005, *MNRAS*, 363, 867.
- Migliari, S., Fender, R.P., Blundell, K.M., Mendez, M., & Van der Klis, M., 2005, *MNRAS*, 358, 860.
- Mirabel, I.F., & Rodriguez, L.F., 1998, *Nature*, 392, 673.
- Mirabel, I.F., & Rodriguez, L.F., 1994, *Nature*, 371, 46.
- Rees, M. J., 1966, *Nature*, 211, 468.
- Smith, D.A., Levine, A., & Wood, A., 1998, *IAU Circular* 6932.
- Rodriguez, L.F. & Mirabel, I.F., 1999, *ApJ*, 511, 398.
- Wex, N., & Kopeikin, S.M., 1999, *Astrophys. J.* 514, 388.
- Whitney, A.R., Shapiro, I.I., Rogers, A.E.E., Robertson, D.S., Knight, C.A., Clark, T.A., Goldstein, R.M., Marandino, G.E., & Vandenberg, N.R., 1971, *Sci*, 173, 225.
- Zhang, S.N., Wilson, C.A., Harmon, B. A., Fishman, G.J., & Wilson, R.B., 1994, *IAU Circular* 6046.

---

This 2-column preprint was prepared with the AAS L<sup>A</sup>T<sub>E</sub>X macros v5.2.

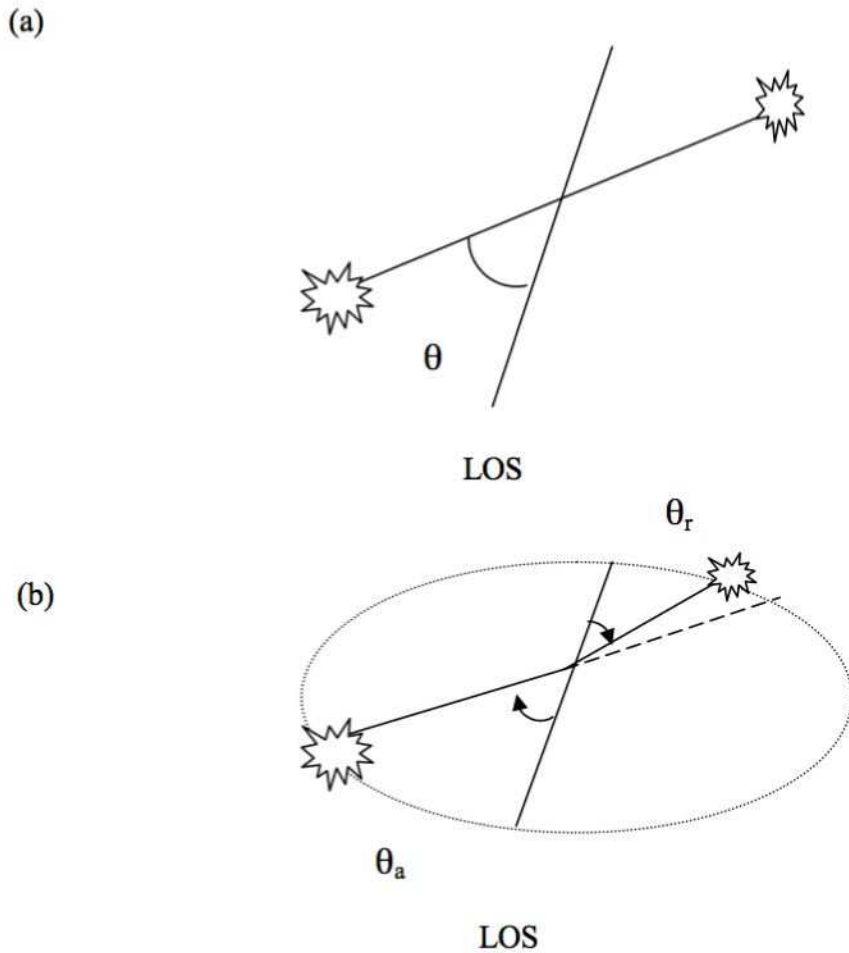


Fig. 1.— A schematic illustrating of the two models on superluminal motion (a) corresponds to the bulk motion model with a constant position angle  $\theta$ . Whereas, the jet precession model corresponds to constant distances from the blobs to the core, and the position angle varies with precession of jet axis.

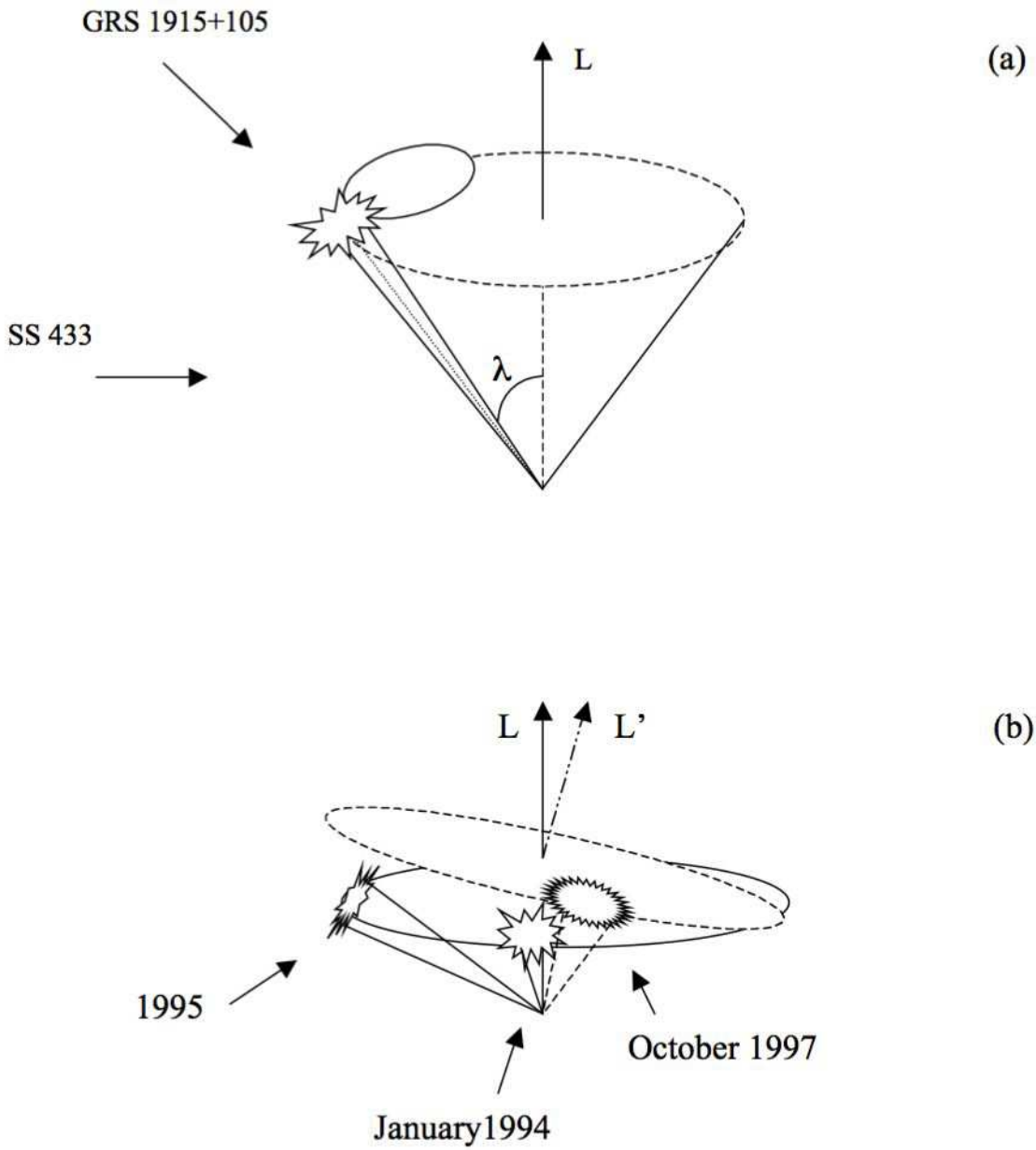


Fig. 2.— A schematic illustrating of the jet precession model. (a) shows that GRS 1915+105 different from SS433 only in the view angle, the former has chance to see the emission corresponding to  $\theta \sim 0$ , whereas the latter never does. The motion of the jet is a primary precession with a opening angle of precession cone,  $\lambda$  (doted ellipse), superimposed by a nutation with small opening angle (solid ellipse). (b) The outburst of January 1994 corresponds to the starting of period of precession. And the outburst of October 1997 corresponds the beginning of another period. The position angle may vary by both short-term effect,  $\sim P_b$ , and long-term effect,  $\sim 3.8$  yr.

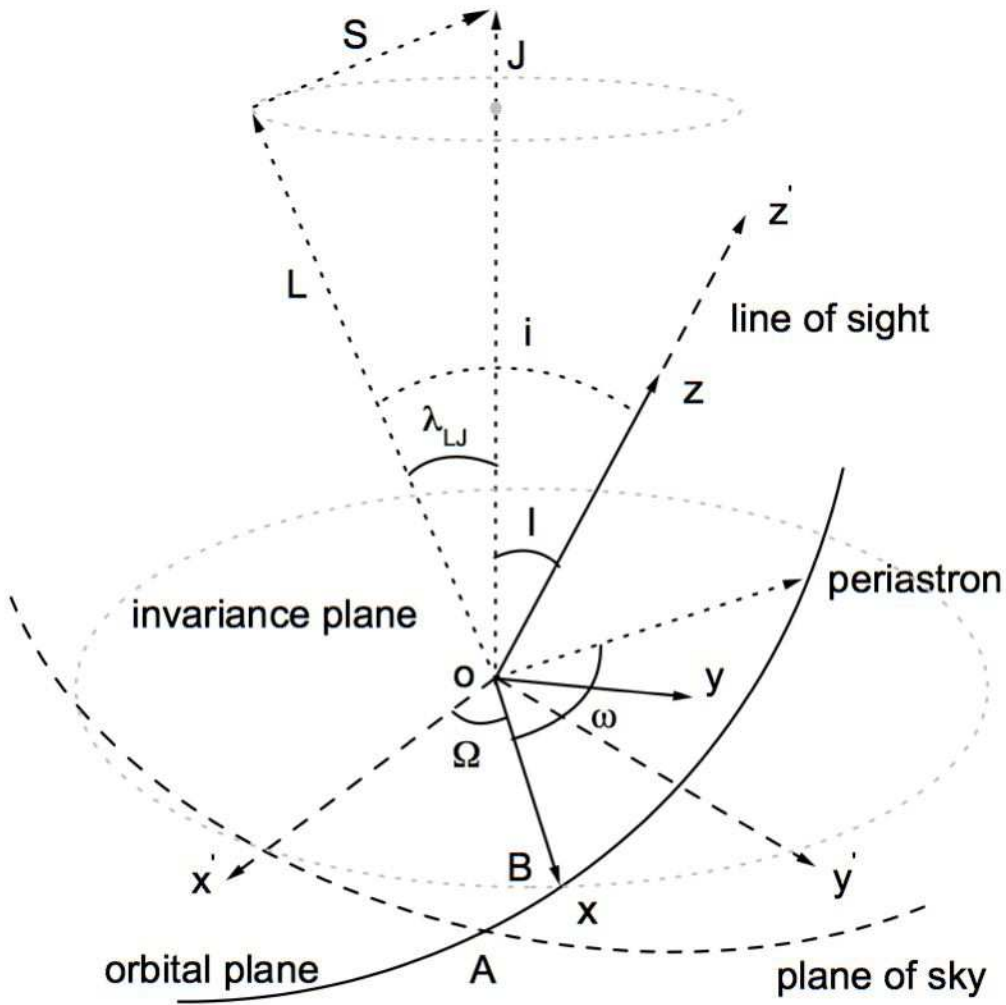


Fig. 3.— Definition of angles and reference frames. The ascending node,  $o - x$ , rotates with respect to the fixed line,  $o - x'$ . The coordinate system,  $x, y, z$  rotates with respect to the static coordinate system,  $x', y', z'$ .

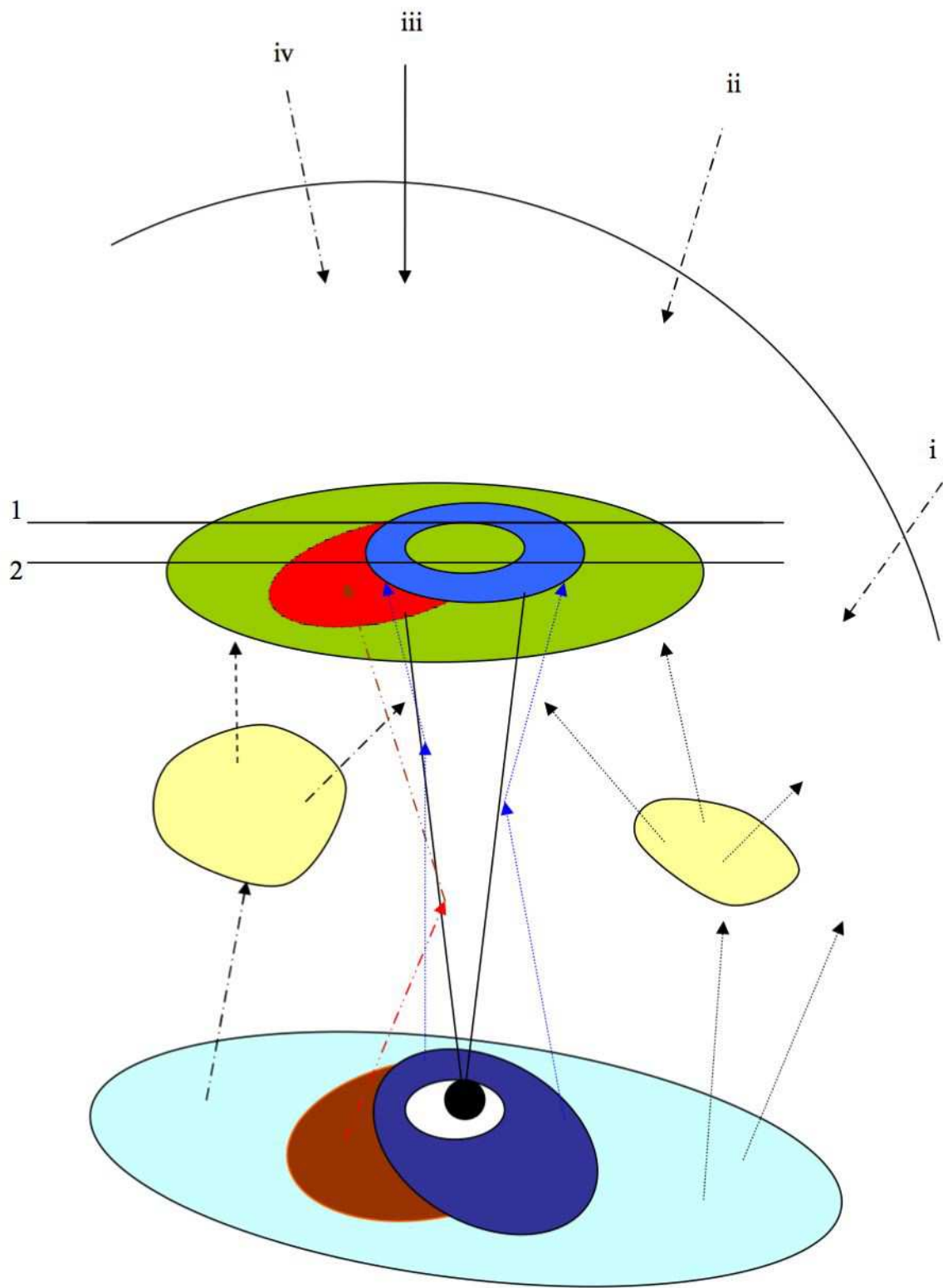


Fig. 4.— A schematic illustrating of the structured jet. The compton scattering of photos from the warped inner regions (blue and brown ellipse) of the disk are beamed and responsible for the state A and B, which can be observed in the case iii and iv. The case *i* corresponds to the quiescent state, the emission is from the disk, the corona (the two volumes between the disk and the beam), wind of the companion star as well as the jet. State ii is a

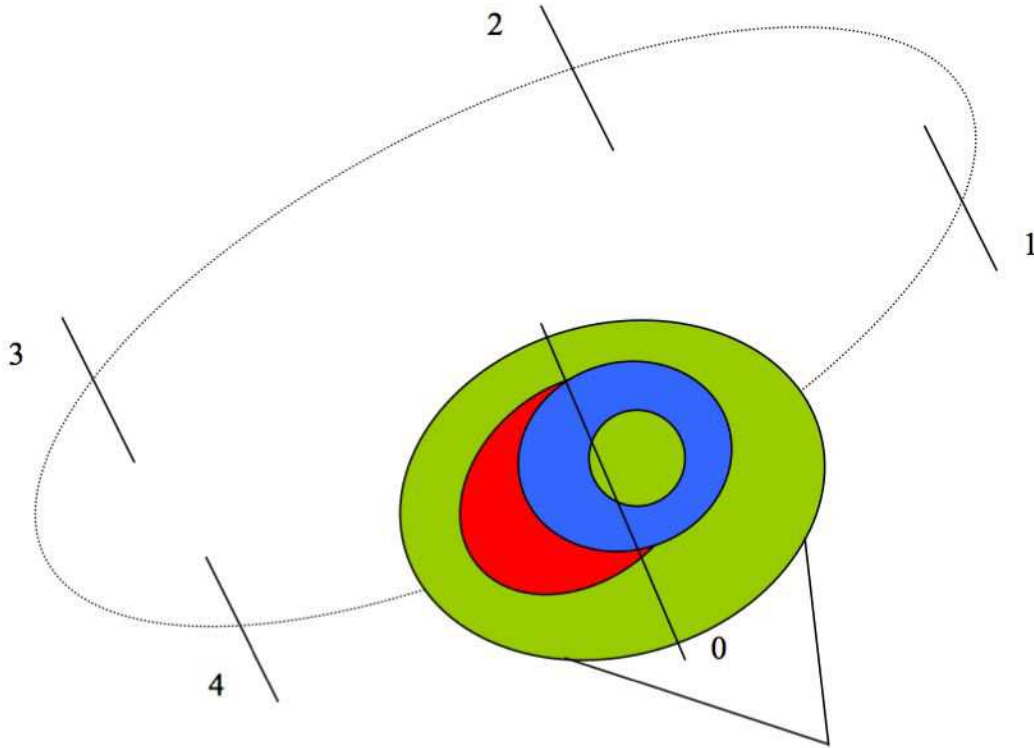


Fig. 5.— A schematic illustrating of the jet precession in a whole period. The label 0 corresponding to  $\theta \sim 0$ , in which high state emission is observed. States 1, 2, 3, 4 correspond to the quiescent states. The long-term primary precession plus the short-term nutation may explain the state evolution of Fender & Belloni (2004).